Final Draft
of the original manuscript:

Tripathi, B.P.; Schieda, M.; Shahi, V.K.; Pereira Nunes, S.:
Nanostructured membranes and electrodes with sulfonic acid functionalized carbon nanotubes
In: Journal of Power Sources (2010) Elsevier

DOI: 10.1016/j.jpowsour.2010.08.110

Nanostructured membranes and electrodes with sulfonic acid functionalized carbon nanotubes

Bijay P Tripathi[1,2], M. Schieda[2], Vinod K Shahi[1*], and Suzana P Nunes[3**]

[1]*Electro-Membrane Processes Division,*
Central Salt and Marine Chemicals Research Institute, Council of Scientific & Industrial Research (CSIR), G.B. Marg, Bhavnagar-364002 (Gujarat) India

[2]*Department of Membranes for Sustainable Energy,*
GKSS Research Centre Geesthacht GmbH, Max Planck Str. 1, D-21502 Geesthacht, Germany

[3]*King Abdullah University of Science and Technology, Thuwal 23955-6900, Kingdom of Saudi Arabia*
suzana.nunes@kaust.edu.sa

Abstract: Herein we report the covalent functionalization of multiwall carbon nanotubes by grafting sulfanilic acid and their dispersion into sulfonated poly (ether ether ketone). The nanocomposites were explored as an option for tuning the proton and electron conductivity, swelling, water and alcohol permeability aiming at nanostructured membranes and electrodes for application in alcohol or hydrogen fuel cells and other electrochemical devices. The nanocomposites were extensively characterized, by studying their physicochemical and electrochemical properties. They were processed as self-supporting films with high mechanical stability, proton conductivity of 4.47×10^{-2} S/cm at 30 °C and 16.8×10^{-2} S/cm at 80 °C and 100 % humidity level, electron conductivity much higher than for the plain polymer. The methanol permeability could be reduced to 1/20, keeping water permeability at reasonable values. The ratio of bound water also increases with increasing content of sulfonated filler, helping in keeping water in the polymer in conditions of low external humidity level.

1. Introduction

The development of materials with advanced nanostructure for energy application has been an issue of increasing relevance. Better carbon-based electrodes are needed for fuel cells [1-2], photocatalyzed water splitting, hydrogen pumps, batteries and other electrocatalytic devices [3]. The requirements for the bulk of fuel cell membranes are mainly high proton conduction, chemical stability and electron insulation [4-8]. However this is only the first step to reach high performance. The electrochemical reaction takes place in the membrane-electrode-catalyst layers and requires high proton and electron conductivity, effective access of reactants to the catalyst, excellent catalyst dispersion, as well as catalyst-polyelectrolyte and polyelectrolyte-electrode adhesion to transport electrons in and out of the reaction site. This layer would profit from advanced nanostructured architectures containing different materials, which could be integrated to address this set of issues. Other emerging electrochemical applications like photocatalyzed water splitting need tuned mixed proton and electron conductivity.

Carbon nanotubes have become an attractive component of electrochemical devices due to (i) their ability of electron conduction, (ii) potentially high surface area, leading to high electrode-electrolyte contact area, (iii) the possibility of being used for catalyst dispersion and deposition and (iv) the high aspect ratio, leading to well directed 1 D conductive path. Perfect alignment can be easily obtained [1,3]. Carbon nanotubes are also becoming less expensive, particularly the multiwall nanotubes. For these and other reasons carbon nanotubes (CNTs) attract much attention as a

new class of advanced ‘‘filler’’ materials with the possibility of employing them in emerging applications in nanoelectronics as well as other nanocomposite applications [9-11].

We here focus more on fuel cell application, but the development could be easily extended to other electrochemical and/or separation applications. Electrodes based on carbon nanotubes are also under investigation for exciting applications as amperometric and bioelectrochemical sensors [12], being quite convenient for direct guiding of electrons towards redox centers in catalytic molecules. Hydrogen fuel cells are those aimed for transport application and currently require materials for high temperature (around 130^{o}C) and low humidity operation. Alcohol fuel cells would be very advantageous for portable application if some technical drawbacks could be overcome to reduce Ohmic losses and enhance their efficiencies during operation [13-16]. Up to now, perfluorosulfonic acid polymers such as Nafion® have been the reference membrane for fuel cell because of their high electrochemical properties as well as excellent chemical resistance [14,17]. However, there is much interest in alternative polyelectrolyte membranes because of Nafion®’s reduced performance above 80 °C and high cost. When considering alcohol fuel cells the alcohol crossover is also excessively high [17-22]. Fluorine free materials with properties comparable to those of Nafion® are one of the directions in the development of cheaper polyelectrolytes. Membranes based on sulfonated aromatic polymers, irradiation graft polymers, cross-linked and blend polymers, were successfully proposed [23-27]. Sulfonated poly (ether ether ketones) (SPEEK) are a

good example. However, to achieve acceptable conductivities, high degree of functionalization is required, which enhances the polymer swelling when hydrated [18,28,29]. This provokes a decrease in mechanical stability and an increase in alcohol crossover. Alternatively, organic-inorganic composite membranes have been prepared by adding inorganic functional entities, such as silica, titania, zirconia, zirconium phosphates, clays, zeolites and Pd metal, into the membranes to reduce methanol crossover in direct methanol fuel cells and to enhance mechanical strength [30-40]. Unfortunately, these composite membranes frequently decrease also the ion conductivity, since the inorganic fillers usually strongly interact with the sulfonic acid group, inhibiting the effective ion transport through membranes.

Functionalized composites of CNTs with Nafion® have been reported and displayed a reduced methanol crossover, but suffer from poor proton conductivities [41]. Moreover, the strong intrinsic van der Waals forces of CNTs as well as the lack of interfacial interactions between CNTs and Nafion® limit the dispersion of CNTs at higher loadings in addition to the load transfer from the Nafion® matrix to the nanotubes. The potential advantages of using CNTs to improve the portfolio performance in polymer fuel cells have therefore not been fully realized, and it is important to enhance the interfacial interactions between the CNTs and polymers in order to obtain a homogeneous dispersion and thus also an enhancement of the properties of the composite membranes. Aromatic condensation polymers such as polyimide [42-44] and polybenzimidazole [45], poly(arylene ether sulfone) [46],

with conjugated groups have been reported to be excellent for dispersing CNTs and enhancing the mechanical properties and were a good starting point for this work.

In this manuscript, for the first time we are reporting the successful development of SPEEK nanocomposites, by mixing the polymer with functionalized MWCNTs obtained by grafting of aromatic sulfonic acid groups.

2. Experimental Section

2.1. Materials

Poly (ether ether ketone) (PEEK) 450 PF powder form was purchased from Victrex and dried under vacuum at 90 ^{o}C over night before use. 4-aminobenzene sulfonic acid, thionyl chloride, and Nafion®117 (perfluorinated membrane) were purchased from Sigma Aldrich Chemicals and used as received. Sulfuric acid 95–97%, tetrahydrofuran (THF), N-methylpyrolidone (NMP) was obtained from Merck, All other chemicals used was of analytical reagent grade from commercial sources. In all experiment double distilled water was used. Non functionalized and carboxyl (COOH) functionalized multiwall carbon nanotubes were provided by Nanocyl.

2.2. Synthesis of organically functionalized MWCNT

The synthesis of sulfonic acid functionalized multiwalled carbon nanotubes (sulf-MWCNT) is shown in Figure 1. The carboxylated MWCNT was treated with 0.1M HCl to convert all carboxylate groups in to carboxylic acid and washed several times with double deionized water until a pH of 7 was obtained. The MWCNT was dried in vacuum oven at 60 ^{o}C for 12h to remove all the absorbed water. Thus

obtained dried carboxylated MWCNT was refluxed with excess and neat thionyl chloride at 65 ^{o}C for 24 h. The residual thionyl chloride was removed by distillation, giving acyl chloride functionalized MWCNT. Further, the acylated MWCNT was dispersed in THF and reacted with 4-aminobenzene sulfonic acid solution in slightly basic medium under refluxing at 60 ^{o}C for 24 h. The resulting sulfonic acid modified MWCNT (sulf-MWCNT) was filtered with Teflon filter paper and washed several times with deionized water. Finally the sulf-MWCNT was dried under vacuum at 60 ^{o}C for 24 h. The functionalization was confirmed by FTIR (supplementary information).

2.3. Membrane preparation

A 5 wt %of SPEEK (sulfonation degree of ca. 50% (IEC = 1.45mequiv./g), sulfonation procedure according to [47]) solution was prepared in NMP and mixed with separately dispersed sulf-MWCNT in NMP under sonication. The SPEEK and sulf-MWCNT mixture was vigorously stirred for 48h and further 6 time sonicated 6 times for 5 min at ambient temperature with intervals of 1 h in between. The amount of sulf-MWCNT was taken as 1, 2, 5, and 10 wt % of SPEEK. All composite solutions were cast on the hydrophobised glass plate and isothermally heated at 65^{o}C for overnight, and dried in vacuum at 80 ^{o}C for 12 h to obtain the nanocomposite membranes. A nanocomposite membrane with unmodified MWCNT with 5 wt% was also prepared for comparison of the results. The SPEEK membrane was prepared as a reference membrane using SPEEK polymer solution. All membranes had an average thickness of 150 μm.

2.4. Measurements and characterizations

2.4.1. NMR spectroscopy

^{1}H NMR spectra were carried out in DMSO on a Bruker 500 MHz spectrometer for the assessment of the interaction between sulf-MWCNT and SPEEK.

2.421. TGA, DSC, and DMA analysis

Thermal degradation and stability of the MWCNT, sulf-MWCNT, and membranes were investigated using a thermogravimetric analyzer (TGA) (Netzsch STA 449C equipment) under a nitrogen atmosphere at a heating rate of 10 ºC /min from 30 to 1000 ºC. Differential scanning calorimetric (DSC) measurements were carried out in a Netzsch 204 DSC, equipped with a TASC 414/2 thermal analysis controller under temperature range of 25 to 400 ºC. The samples of about 10 to 20 mg were loaded into aluminum pans, and then heated to the desired temperature with the heating rate of 10 ºC /min. The empty aluminum pan was used as a reference during the course of experiment. The dynamic mechanical stability of the composite membranes was evaluated by using a dynamic mechanical analyzer (Mettler Toledo; DMA) 861^{c} instrument with Star^{c} software under a nitrogen atmosphere with a heating rate of 10 ºC /min from 30 to 450 ºC to verify the effect of CNT content on membrane mechanical stability.

2.4.3. Microscopic characterizations

The membrane samples were fractured in liquid nitrogen, coated with Au/Pd by sputtering and investigated in FEI Quanta 200 field emission scanning electron microscope.

2.4.4. Water uptake and state of water

The uptake of water and water-methanol solution as well as the state of water in the membrane were measured according to procedure described in the supplementary information.

2.4.5. Pervaporation and methanol permeability

Pervaporation experiments were performed according to the procedure described elsewhere [48], additional details in supplementary information] using solution of 5% methanol-water at 55 ^{o}C, a total pressure of 1bar on the feed side and a vacuum (10^{-2} mbar) on the permeate side. The effective membrane area (the area accessible for the feed mixture after the membrane is sealed in the measurement cell with Viton® O-ring) was 12.5 cm^2. Prior to the pervaporation experiments, the membranes were conditioned in the feed solution over night. After the establishment of a steady state, permeate was collected for 1h in cooled traps immersed in liquid nitrogen. The compositions of feed and permeate were determined by gas chromatography using a Hewlett Packard 5890 chromatograph equipped with a HP-PLOUT-U capillary column (30m×0.53mm×1.0um film thickness) and using an oven temperature of 280 ◦C and flame ionization detector at 280 ◦C.

2.4.6. Proton and electron conductivity

Proton conductivity measurements for the composite membranes were carried out in water (after equilibration with 0.01M HCl for 24 h) using a potentiostat/ galvanostat

frequency response analyzer (Auto Lab, Model PGSTAT 30). The membranes were sandwiched between two in-house made circular stainless steel electrodes (4.0 cm^2). Within a frequency range of 10^6 to 1 Hz, sinusoidal alternating currents (AC) were supplied to the respective electrodes at a scanning rate of 1 μA/s and sinusoidal potential response was measured. The spectrum of the blank short-circuited cell was also collected and this data was subtracted (as a series circuit) from each of the recorded spectra of the membranes to eliminate cell and wiring resistances and inductances. The corrected spectra were viewed as complex impedance plots with the imaginary component (*Z''*) of Zon the y-axis and the real component (*Z'*) on the x-axis ($Z = Z' - iZ''$); the ionic resistance of each membrane was estimated to be the intersection of the x-axis with the extrapolation of the low frequency linear component of each plot. The membrane resistances were obtained from Nyquist plots and the proton conductivity (κ^m) was calculated from Eq. (1):

$$\kappa^m\left(S/cm\right) = \frac{L(cm)}{R(\Omega) \times A\left(cm^2\right)} \qquad (1)$$

where *L* is the distance between the electrodes used to measure the potential, *R* is the resistance of the membrane, and *A* is the surface area of the membrane.

The electronic conductivity of the dry membranes with various amounts of CNTs was measured with four probes DC conductivity meter (Scientific Equipment & Services, Roorkee, India).

3. Result and discussion

3.1. Functionalization of MWCNT and membrane preparation

Sulfonic acid functionalized MWCNT was synthesized in two steps; in first step, carboxylic acid group was converted into acyl chloride group by refluxing with thionyl chloride under heated condition, and in the second step, the acylated MWCNT was reacted with 4-aminobenzene sulfonic acid solution in slightly basic medium at 60 ^{o}C. In this way, a macroscopically homogeneous dispersion was obtained in THF and was stable for several days. The sulfonation of MWCNT was confirmed by FTIR (supplementary information). TGA was used for quantitative characterization of sulfonic acid groups present in sulf-MWCNT. TGA thermograms of MWCNT and sulf-MWCNT are presented in Figure 2. The amount of the sulfonate moiety of the sulf-MWCNT was determined by using a weight loss difference between pristine MWCNT and sulf-MWCNT at 675 ^{o}C [49]. The calculated sulfonate content was found to be about 8 wt%, which indicated the method applied in this work is effective for functionalization of CNTs. The dispersion of sulf-MWCNT and pristine CNTs was made in NMP by sonicating for 30 min.

The SPEEK-sulf-MWCNT membranes with different compositions of nanotubes (1-10 wt%) were prepared by solution blending in NMP by dispersion method. The stability of the dispersion was studied through a centrifugation test. After being subjected to a centrifugation test at 10,000 rpm for 30 min, all sulf-MWCNTs were found to remain in solution. This observation suggested that SPEEK was bonded to CNTs via ionic and molecular interaction and both components have good

miscibility to each other. Further, sulf-MWCNT-SPEEK dispersion was also investigated by ^{1}HNMR spectroscopy. Figure 3 shows ^{1}HNMR spectra of SPEEK and sulf-MWCNT-SPEEK (1:8 mass ratios) dispersion in DMSO-d^{6}. A broadening of the peaks was observed and the intensity was reduced compared to SPEEK. Previous study also showed that a broadening of proton peaks and reduced intensity for the polymer after dispersion of CNTs [50]. This evidence strongly supported that there was good interaction between the sulf-MWCNT and SPEEK matrix. The sulf-MWCNT dispersion in NMP after sonication was mixed with SPEEK solution in NMP. The mixture was further stirred and sonicated for 30 min and transformed into thin film. The dried membranes were conditioned in acid and base followed by washing with deionized water and stored in wet condition. The polymer electrolyte membranes applications, the mass ratio of sulf-MWCNT/SPEEK was controlled up to 10% in order to avoid any short circuiting in the fuel cell. Casting of the dispersions on a hydrophobized glass substrate and successive drying at 65^{o}C for 24 h and at 90^{o}C in vacuum for 12 h provided homogeneous composite membranes.

3.2. Thermal stability and mechanical properties.

TGA was used to characterize the incorporation of sulf-MWCNT into SPEEK. Figure 4 shows the TGA curve of the sulf-MWCNT-SPEEK referenced composite membranes. In the curve corresponding to the composite membrane, three step weight losses could be observed over the temperature ranges 50–150, 150–300 and 500– 750 C. Similar results were seen in the curve of the pristine SPEEK membrane [51]. The first weight loss was assigned to the evaporation of hydrated water and the

second to the decomposition of the sulfonic acid groups. The nanocomposite membranes show the higher degradation temperature than that of SPEEK. The on-set decomposition temperature for the second step of the sulf-MWCNT/SPEEK composite membranes was approximately 30 ^{o}C higher than that of its pristine SPEEK counterpart. The last weight loss, which started around 500 ^{o}C, was attributed to the decomposition of the polymer backbone. Thus, the TGA results also confirmed the existence of a molecular-level interaction between SPEEK and the sulf-MWCNT. The thermal stability of the nanocomposite membranes also depends on the glass transition (T_g) temperature. The DSC thermograms of the corresponding membranes are presented in Figure 5.The T_g of the SPEEK membrane is at 149 ^{o}C while that of nanocomposite membranes are in the high range of 158–165 ◦C. The increase of glass transition temperature also revealed the interaction between the nanotubes and SPEEK matrix. Moreover, the mechanical stability of the membranes was evaluated via the dynamic mechanical analysis (Figure 6). The storage modulus was increased with the increase of sulf-MWCNT concentration and the highest was 5016 MPa for the SPEEK-sulf-MWCNT-10 membrane. It should be noted that when the sulf-MWCNT content increases, it gives only small effect to thermal stability (TGA and DSC) whereas it improves mechanical stability significantly.

3.3. Microscopic characterizations

The morphology of the nanocomposite membranes fractured in liquid nitrogen was studied by field emission scanning electron microscopy. Figure 7 clearly shows how the adhesion between the carbon nanotubes and the SPEEK matrix is improved

with the functionalization. The distribution of CNTs in the SPEEK matrix is quite uniform but in Fig. 7a the nanotubes are well detached from the matrix, while in the other membranes with functionalized fillers practically no cavities between filler an matrix are observed. [52]. A very dense structure is observed at higher contents of carbon nanotubes and this is reflected also in the permeation characteristics of the membrane, as seen below.

3.4. Uptake and dimensional stability in water and water-methanol mixture

The water uptake in a proton-conducting membrane is an important factor that directly affects proton transportation in proton-conducting membranes. Generally, it is believed that protons can be transported along with cationic mixtures such as H_3O^+ and H_5O^{2+} in the aqueous medium. In a fully hydrated state, sulfonated polymers may dissociate immobile sulfonic acid groups and mobile protons in aqueous solution. Then the free protons move through a localized ionic network within fully water-swollen sulfonated polymer membranes. Accordingly, an appropriate water content level should be maintained in sulfonated polymer membranes to maintain high proton conductivity. The measured water uptakes of the functionalized SPEEK-sulf-MWCNT membranes along with SPEEK (at 30 °C), after equilibration in water for 24h, are compared in Table 1. It is worth noting that all the composite membranes have lower water uptakes than SPEEK. One might ascribe this lower water uptake to the lower IEC value (obtained as described in the supplementary information) of the composite membrane (Table 2). However, Membranes with 5% and 10% sulf-MWCNT loading have IEC values of 1.78 and 1.84 mequiv/g, respectively, which are close to, that of SPEEK. An explanation is that the adhesion

between sulf-MWCNT and polymer is strong. SPEEK is confined between adjacent nanotubes, which hinder swelling. The number of water molecules per ionic sites was also calculated (Table 1) and decreased with increasing sulf-MWCNT concentration. This easy to understand, since by adding nanotubes the content of sulfonic functional groups increases due to the functionalization, but at the same time water uptake decreases.

Water-methanol uptake nature of the membranes was also studied and the related data are also compared in Table 1. It was noticed that, the water-methanol uptake was much higher than that of the water uptake for all the membranes. However the uptake followed the same trends as was observed for water uptake.

The dimensional changes of all membranes were evaluated by measuring the total volume expansion (ϕ_v, %) at room temperature, as reported in Table 1. Change in the dimensions due to swelling was found to be almost the same in all directions (isotropic swelling).ϕ_v values decreased with increasing sulf-MWCNT content, due to the lower water uptake and to the formation of the robust scaffold that was produced by the incorporated sulf-MWCNT.

3.5. State of water and water retention capacity

Water sorption characteristics are of great importance for proton-conducting polymer membranes. According to the Eikerling's theory, PEMs posses two types of water: bound water and the bulk water [53]. Bound water required for the solvation of the sulfonic acid groups, while bulk water fills the void volume. The states of water in sulfonated polymers directly affect the transportation of protons across the

membranes. All the samples had a broad endothermic peak in the DSC. The freezable water peaks including free water were observed at 2.5 °C for plain SPEEK membrane. The membranes with sulf-MWCNT showed a slightly lower melting point due to the increasing percentage of bound water.

The weight fraction of free water (φ_f) in the fully hydrated membranes can be estimated from the total melting enthalpy (ΔH_m) that is obtained by integration of the transition heat capacity (ΔC_P) over the broad melting temperature interval in

$$Free\ water\ (\varphi_f) = \frac{\Delta H_m}{Q_{melting}} = \int \frac{\Delta C_p dT}{Q_{melting}} \qquad (2)$$

where $Q_{melting}$ is the heat of fusion of bulk ice (334 J/g). The weight fraction of free water was converted into the number of free water molecules per ionic sites (λ_f). The number of bound water per ionic sites (λ_b) was calculated by subtracting the λ_f from the total number of water molecules per ionic sites λ_w. Then the bound water degree ($\chi = \lambda_b/\lambda_w$) was calculated from the ratio of the number of bound water to the total water per ionic sites. Table 1 also summarizes the number of freezing and bound water molecules and the corresponding bound water degree. For sulf-MWCNT-SPEEK composite membranes, an increase in sulf-MWCNT concentration resulted in a decrease in λ_f. Composite membrane also contained other polar functional groups such as the -SO_3H, -NH- and –CO-NH- groups from the modified MWCNT surface. In addition to the strong interaction between the water and the

sulfonic acid groups, there are enough binding sites in the membranes to constrain water on the MWCNT sidewalls and thus bring about a high λ_b.

Water vapor sorption and diffusion properties of developed composite membranes have significant effects on conductivity and their use at high temperature under low humidity. The water retention capability ((M_t/M_o)-*t* (time) curves) was illustrated in Figure 8. The effect of CNTs inclusion in membrane was clearly reflected in the desorption profile of the membranes. Water desorption kinetics was further evaluated by plotting (M_t/M_0-$t^{1/2}$) as a function of time and calculating the water desorption coefficient based on the Higuchi's model [52] (Table 1). Rate of water desorption was reduced with the increase of CNT content. Thus, sulf-MWCNT acted as water binder in the membrane matrix. The free water in ionic membrane matrix becomes less mobile. Water being more bound to the hydrophilic domains becomes less susceptible to dehydration. Thus, sulf-MWCNT hinders water release and improves the water retention capacity even at higher temperature.

3.6. Pervaporation and methanol permeability

The water uptake and its interaction with the nanocomposite film have a direct influence on the permeability characteristics of the membrane. The permeability was investigated with pervaporation experiments, by measuring the performance of the nanocomposite membranes for water and methanol permeation at 55 ^{o}C. To analyze the permeation behavior of each component (methanol and water), individual membrane permeability values are given in Table 1.

The membrane permeability (P_{Water} and P_{MeOH}) depends on the nature of the membrane forming material and on the operating conditions, such as temperature, feed composition, pressure etc. When carbon nanotubes are added to the membrane, they reduce the permeability both for methanol and water. However without functionalization the weak adhesion between polymer matrix and nanofillers give rise to cavities, which favor molecular diffusion. With the functionalization, the membranes void volume is reduced, leading to much slower diffusion of the penetrants and low permeability. P_{Water} and P_{MeOH} were both decreased with the increase of functionalized nanotubes. However the decrease of water permeability was much less evident compared to that of methanol. Although the diffusion is hindered by the nanotubes, water solubility is stimulated by the increase of concentration of hydrophilic sulfonic sites, as confirmed by IEC values discussed below. P_W values were about 100 times higher than $P_{MeOH.}$ It is well known that separation characteristics of a membrane depend upon the interaction between species to be separated and membrane matrix. Hydrophilic membrane like functionalized SPEEK-sulf-MWCNT nanocomposite can develop hydrogen bond interaction with water leading to preferential sorption and permeation of water through the membrane [54]. Table 1 also summarized the selectivity of the water and methanol with the prepared membranes. $\alpha_{water/methanol}$ for SPEEK was about 74, however for SPEEK-sulf-MWCNT-10, was about 602.

From these results it can be observed that SPEEK-sulf-MWCNT nanocomposite membranes are highly suitable for water-methanol dehydration as well as excellent candidates for the application in alcohol fuel cells.

3.7. IEC and proton conductivity

The IEC depends on the density of functional groups and is crucial for water uptake and proton conductivity. The IEC values (Table 2) clearly decreased when non-functionalized carbon nanotubes were added to the membrane. The decrease was much higher than expected taking in account only the weight of non-sulfonated component. The carbon nanotubes therefore are reducing also the access to polymer functional groups. However with the functionalization the IEC values are partially recovered and increase with increasing concentration of functionalized CNT. Among the prepared composite membranes, SPEEK-sulf-MWCNT-10had an IEC value of1.84 mequiv./g, which is higher than Nafion®117 membranes.

Acidic functional groups (-SO_3H) of composite polyelectrolyte membranes dissociate due to hydration and allow transport of hydrated proton (H_3O^+). The proton conductivity was measured from 30 to 80 °C for hydrated membranes and data for 30 ^oC are presented in Table 2. The temperature dependence of proton conductivity (κ^m) of all membranes is shown in Figure 9. The change of conductivity with temperature was consistent with the Arrhenius relationship for all the composite membranes. The activation energy varied from 24.2 kJ mol^{-1} for a membrane with 10 wt % functionalized nanotubes to 26.8 kJ mol^{-1} for the plain SPEEK membrane. The interaction between the functional groups of CNT and polymer provided effective hydrated ionic paths. As mentioned before the T_m of water in composite membrane was slightly lower than that in SPEEK. This indicates that the interaction between water and composite membrane was stronger than that between water and

SPEEK. The nanocomposite was capable of maintaining bound water as the temperature was raised, resulting in higher proton conductivity compared to that of SPEEK, particularly at high temperature. Also the ratio of bound water for the composite membranes was higher compared to that of SPEEK. This makes the material not only useful for alcohol fuel cell but also for hydrogen polymer fuel cell operating above 100^{o}C. The protonic transport occurs via a mixture of both Grotthuss- and vehicle-type conduction, where polyatomic molecules such as $H_{2n+1}O_n^+$ are the dominant charge carriers and play a role different from that in the Grotthuss-type mechanism.

3.9 Electron conductivity

The use of carbon nanotubes to add electron conductivity to polymer insulators is well known [55] and can be achieved with very small loading, as soon as the percolation threshold is overcome. Threshold as low as 0.002 vol. % have been reported for multi-wall nanotubes. At the threshold a conductivity jump is observed. The conductivity values depend not only on the composition, but on the nanotube characteristics itself, like aspect ratio and surface functionalization, as well as on dispersion quality and alignment. Table 2 shows how electron conductivity changes with the addition of the sulfonated nanotubes developed in this paper. The addition of the non-functionalized carbon nanotubes led to a jump in conductivity. After functionalization the increase of conductivity relative to the pristine SPEEK was up to 17-fold, but this value is much lower than that obtained without the functionalization. The electrical property of CNT is known to be very dependent on

structural changes caused by chemical treatment [56]. When sp^3 carbon bonds are formed the π–conjugation responsible for high electron conductivity is partially disturbed.

4. Conclusion

Figure 10 summarizes the influence of carbon nanotubes on different membrane properties relevant for electrochemical application. As the functionalized filler content increases to 5-10 wt % the following effects were obtained:

- Slight increase of proton conductivity;
- Jump in electron conductivity;
- Reduction of methanol permeability down to 1/20 of the value for plain SPEEK;
- Reduction of water permeability only down to 1/3 of the value for plain SPEEK

These are very convenient achievements when aiming at electrochemical applications. A good example is the case of alcohol fuel cells. When developing optimized cathodes, the catalyst must be protected from the contact with alcohol. However water transport is necessary to avoid catalyst flooding as the fuel cell operation proceeds, producing water. Transport of water to other parts of the membrane can thus keep it humidified, retaining proton conductivity at a high level. Protons must reach the reactive site and this is assured by high proton conductivity. The electrochemical reaction can only take place on the catalyst surface if enough electron conductivity is present. An optimized alcohol fuel cell device might be therefore constituted by at least two layers: an electron insulating polymer layer of

high proton conductivity and a layer with functionalized carbon nanotubes on the cathode side.

The development was possible by first grafting sulfonic acid groups on MWCNTs and effectively dispersing them in proton conductive SPEEK matrix. The homogeneous dispersion occurred primarily via π-π and functional group interactions.

When considering hydrogen fuel cells operating above 100^{o}C and low external humidity, the increase of bound water at higher content of functionalized MWCNT is very advantageous.

The mechanical stability of the membrane is also increased with the introduction of functionalized MWCNT and swelling is reduced.

In summary by tuning the composition and functionalization of carbon nanotubes, the resulting nanocomposites with mixed electron and proton conductivity can useful not only as membrane-electrodes for fuel cell, but also for other emerging electrochemical applications such as hydrogen pumps, sensors and water splitting.

Acknowledgement:

The authors thank Dr. Lan Zhao for helping with the microscopy. The work of B. P. Tripathi at GKSS was supported by DAAD.

Reference

1. K. Prehn, R. Adelung, M. Heinen, S. P. Nunes, K., J. Membr. Sci., 321 (2008) 123-130.
2. H. Maab, S. Shishatskiy, S. P. Nunes, J. Membr. Sci., 326 (2009) 27-35.
3. G. Centi and S. Perathoner, Catalysis Today, 150 (2010) 151-162.
4. H. Maab, M. Schieda, W. Yave, S. Shishatskiy, S. P. Nunes, Fuel Cells, 9 (2009) 401-409.
5. P. Totsatitpaisan, S. P. Nunes, K. Tashiro, S. Chirachanchai, Solid State Ionics, 180 (2009) 738-745.
6. S. H. Pezzin, N. Stock, S. Shishatskiy, S. P. Nunes, J. Membr. Sci., 325 (2) (2008) 559-569.
7. M. L. Ponce, D. Gomes, S. P. Nunes, J. Membr. Sci., 319 (2008) 14-22.
8. H. Maab, S. P. Nunes, J. Power Sources, 195 (2010) 4036-4042.
9. R. Andrews, D. Jacques, D. Qian, T. Rantell, Acc. Chem. Res., 35 (2002) 1008–1017.
10. Y. P. Sun, K. Fu, Y. Lin, W. Huang, Acc. Chem. Res., 35 (2002) 1096–1104.
11. P. M. Ajayan, Chem. Rev., 99 (1999) 1787–1800.
12. K. Balasubramanian, M. Burghard, Small, 1 (2005) 180-192.

13. A. Siu, J. Schmeisser, S. Holdcraft, J. Phys. Chem. B, 110 (2006) 6072–6080.
14. F. Pereira, K. Valle, P. Belleville, A. Morin, S. Lambert, C. Sanchez, Chem. Mater., 20 (2008) 1710-1718.
15. J. A. Kerres, J. Membr. Sci. 185 (2001) 3-27.
16. J. Y. Kim, W. C. Choi, S. I. Woo, W. H. Hong, J. Membr. Sci., 238 (2004) 213-222.
17. P. Costamagna, S. Srinivasan, J. Power Sources, 102 (2001) 242-252.
18. M. A. Hickner, H. Ghassemi, Y. S. Kim, B. R. Einsla, J. E. McGrath, Chem. Rev., 104 (2004) 4587-4612.
19. B. R. Einsla, Y. S. Kim, M. A. Hickner, Y. T. Hong, M. L. Hill, B. S. Pivovar, J. E. McGrath, J. Membr. Sci., 255 (2005) 141-148.
20. T. Prabhuram, T. S. Zhao, Z. X. Liang, H. Yang, C. W. Wong, J. Electrochem. Soc., 152 (2005) A1390-A1397.
21. M. S. Kang, J. H. Kim, J. Won, S. H. Moon, Y. S. Kang, J. Membr. Sci., 247 (2005) 127-135.
22. Q. Li, R. He, J. O. Jensen, N. J. Bjerrum, Chem. Mater., 15 (2003) 4896-4915.
23. H. Ghassemi, G. Ndip, J. E. McGrath, Polymer, 45 (2004) 5855-5862.
24. X. Zhang, S. Liu, L. Liu, J. Yin, Polymer, 46 (2005) 1719-1723.
25. V. K. Shahi, Solid State Ionics, 177 (2007) 3395-3404.
26. P. Xing, G. P. Robertson, M. D. Guiver, S. D. Mikhailenko, S. Kaliaguine, Macromolecules, 37 (2004) 7960-7967.

27. L. Depre, M. Ingram, C. Poinsignon; M. Popall, Electrochimica Acta, 45 (2000) 1377-1383.
28. J. Kerres, W. Zhang, W. Cui, J. Polym. Sci., Part A: Polym. Chem., 36 (1998) 1441-1448.
29. V. V. Binsu, R. K. Nagarale, V. K. Shahi, J. Mater. Chem., 15 (2005) 4823-4831.
30. P. Dimitrova, K. A. Friedrich, B. Vogt, U. Stimming, J. Electroanal. Chem., 532 (2002) 75–83.
31. H. Y. Chang, C. W. Lin, J. Membr. Sci., 218 (2003) 295–306.
32. B. P. Ladewig, R. B. Knott, A. J. Hill, J. D. Riches, J. W. White, D. J. Martin, J. C. D. daCosta, G. Q. Lu, Chem. Mater., 19 (2007) 2372–2381.
33. S. P. Nunes, B. Ruffmann, E. Rikowski, S. Vetter, K. Richau, J. Membr. Sci., 203 (2002) 215–225.
34. V. S. Silva, S. Weisshaar, R. Reissner, B. Ruffmann, S. Vetter, A. Mendes, L. M. Madeira, S. P. Nunes, J. Power Sources, 145 (2005) 485–494.
35. F. Bauer, M. Willert-Porada, J. Membr. Sci., 233 (2004) 141–149.
36. C. W. Lin, R. Thangamuthu, C. J. Yang, J. Membr. Sci., 253 (2005) 23–31.
37. D. H. Jung, S. Y. Cho, D. H. Peck, D. R. Shin, J. S. Kim, J. Power Sources, 118 (2003) 205–211.
38. C. H. Rhee, H. K. Kim, H. Chang, J. S. Lee, Chem. Mater., 17 (2005) 1691–1697.
39. B. Libby, W. H. Smyrl, E. L. Cussler, AIChE J., 49 (2003) 991–1001.

40. C. Pu, W. Huang, K. L. Ley, E. S. Smotkin, J. Electrochem. Soc., 142 (1995) L119–L120.
41. J. M. Thomassin, J. Kollar G. Caldarella, A. Germain, R. Jerome, C. Detrembleur. J. Membr. Sci., 303 (2007) 252-257.
42. H. Chen, Z. Liu, P. Cebe, Polymer, 50 (2009) 872-880.
43. D. M. Delozier, K. A. Watson, J. G. Smith, T. C. Clancy, J. W. Connell, Macromolecules, 39 (2006) 1731-1739.
44. L. Licea-Jimenez, A. D. Grishina, L. Y. Pereshivko, T. V. Krivenko, V. V. Savelyev, R. W. Rychwalski, et al., Carbon, 44 (2005) 113-120.
45. M. Okamoto, T. Fujigaya, N. Nakashima, Adv. Funct. Mater., 18 (2008) 1776-1782.
46. S. H. Zoo, C. Pak, E. A. Kim, Y. H. Lee, H. Chang, D. Seung, Y. S. Choi, J. B. Park, T. K. Kim, J. Power Sources, 180 (2008) 63-70.
47. S. Vetter, B. Ruffmann, I. Buder, S. P. Nunes, J. Membr. Sci. 260 (2005) 181-186.
48. A. Dyck, D. Fritsch, S. P. Nunes, J. Appl. Polym. Sci., 86 (2002) 2820–2827.
49. S. H. Zoo, C. Pak, E. A. Kim, Y. H. Lee, H. Chang, D. Seung, Y. S. Choi, J. B. Park, T. K. Kim, J. Power Sources 180 (2008) 63-70.
50. N. Li, F. Zhang, J. Wang, S. Li, S. Zhang, Polymer, 50 (2009) 3600-3608.
51. R. Gosalawit, S. Chirachanchai, S. Shishatskiy, S. P. Nunes, J. Membr. Sci., 323 (2008) 337–346.
52. D. Gomes, M. R. Loos, M. H. Wichmann, A. De, K. Schulte, Composites Sci. Techn., 69 (2009) 220-227.

53. M. Eikerling, A. A. Kornyshev, U. Stimming, J. Phys. Chem. B, 101 (1997) 10807-10820.
54. D. A. Devi, B. Smitha, S. Sridhar, T. M. Aminabhavi, J. Membr. Sci., 262 (2005) 91-99.
55. M. Moniruzzaman and K. I. Winey, Macromolecules 39 (2006) 5194-5205.
56. Q. Li, X. Zhang, S. B. Chikkannanavar, Y. Zhao, A. M. Dangelewicz, L. Zheng, S. K. Doorn, Q. La, D. E. Peterson, P. N. Arendt and Y. Zhu, Adv. Materials, 19 (2007) 3358-3363.
57. B. P. Tripathi, V. K. Shahi, J. Phys. Chem. B, 112 (2008) 15678-15690.
58. B. P. Tripathi, V. K. Shahi, ACS Appl. Mater. Interf., 1 (2009) 1002-1012.
59. T. Y. Liu, S. Y. Chen, Y. L. Lin, D. M. Liu, Langmuir, 22 (2006) 9740-9745.

Table 1

Table 1. Solvent uptake, dimensional stability, number of water molecules per ionic sites (free and bound), enthalpy of melting, water diffusion coefficient of the nanocomposite membranes.

wt % sulf-MWCNT in SPEEK membranes	φ_w (wt %)	φ_{w+MeOH} (wt %)	ϕ_v (vol %)	λ_w /ionic site	λ_f	λ_b	ΔH_m (J g^{-1})	D (10^{-6} cm^2 s^{-1})	P (10^{-8} kg m s^{-1} m^{-2})	
									water	*methanol*
0	27.5	34.2	95	7.49	0.68	6.81	8.33	8.38	15.5	0.210
5*	17.2	22.8	82	8.31				8.39	10.8	0.197
1	19.8	24.4	78	6.79	0.62	6.17	6.01	5.59	12.3	0.022
2	20.2	26.7	69	6.80				------	6.5	0.018
5	21.4	27.5	63	6.68	0.54	6.14	5.07	4.57	6.6	0.016
10	22.5	28.3	59	6.79	0.42	6.37	4.65	4.21	5.7	0.010

**non-functionalized*

Table 2

Table 2. Ion-exchange capacity, proton and electronic conductivity.

wt % sulf-MWCNT in SPEEK membrane	*IEC* (mequiv.g^{-1})	*Proton conductivity* (10^{-2} S cm^{-1})	*Electron conductivity* (10^{-8} S cm^{-1})
0	2.04	2.51	0.0053
5*	1.15	1.82	16.1
1	1.62	3.59	0.0261
2	1.65	3.62	0.0308
5	1.78	3.78	0.0593
10	1.84	4.47	0.0882

**non-functionalized*

Figure 1
Click here to download Figure(s): Figure 1.docx

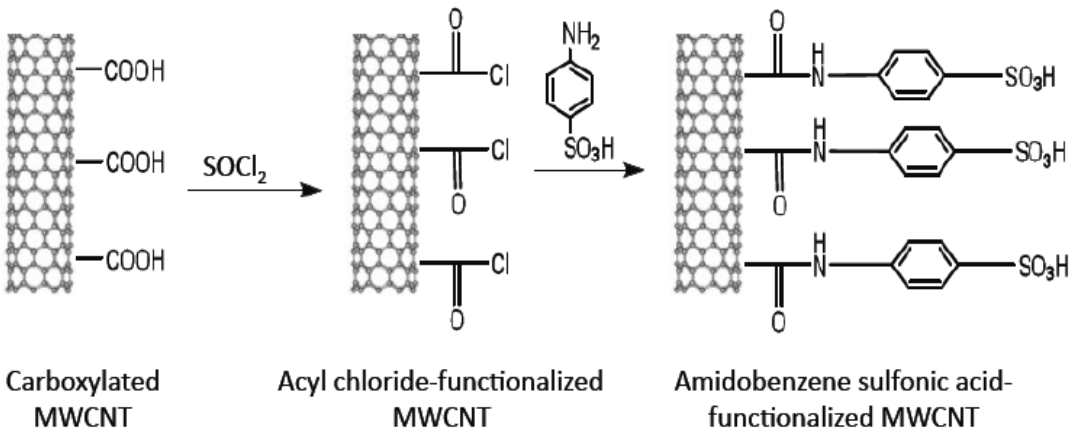

Figure 1. Schematic reaction route of the surface functionalization of MWCNT.

Figure 2
Click here to download Figure(s): Figure 2.docx

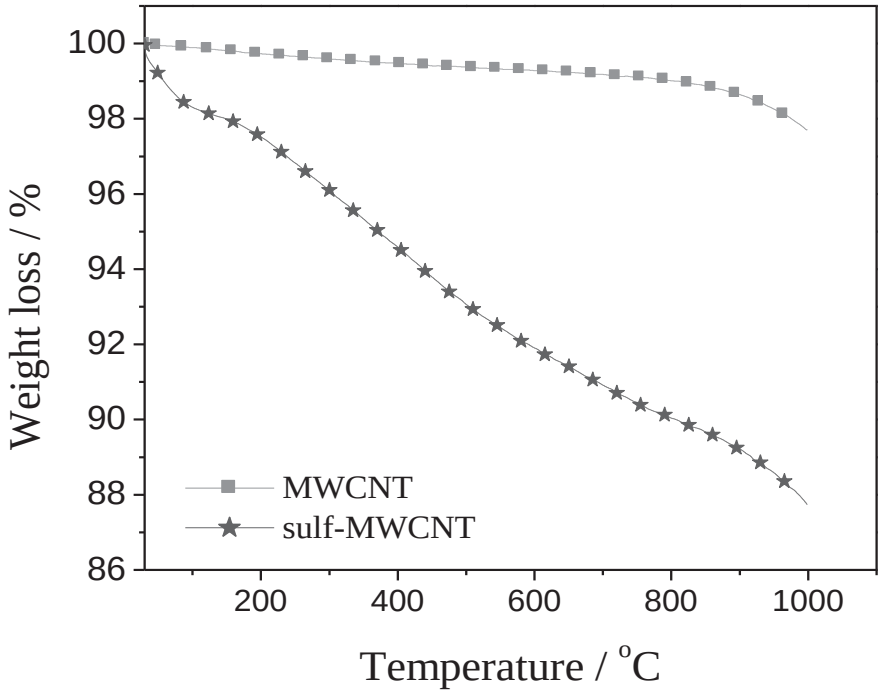

Figure 2. Weight loss characteristic of unmodified and modified MWCNT.

Figure 3
Click here to download Figure(s): Figure 3.docx

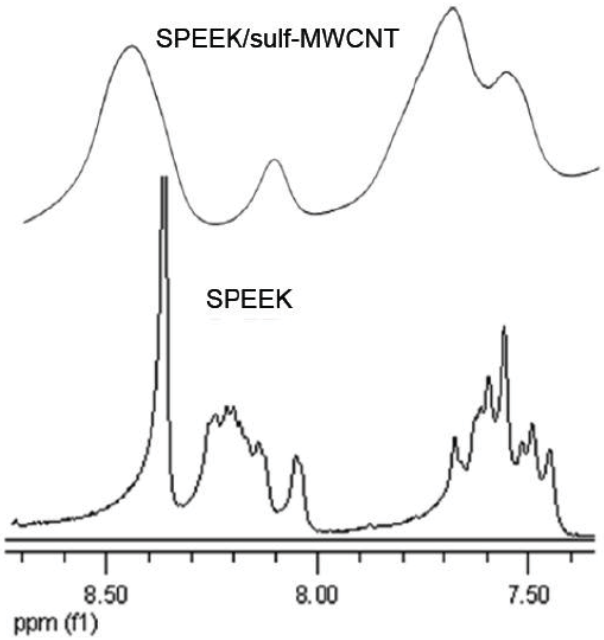

Figure 5. Peak broadening in ^{1}H NMR after mixing of sulf-MWCNT in SPEEK.

Figure 4
Click here to download Figure(s): Figure 4.docx

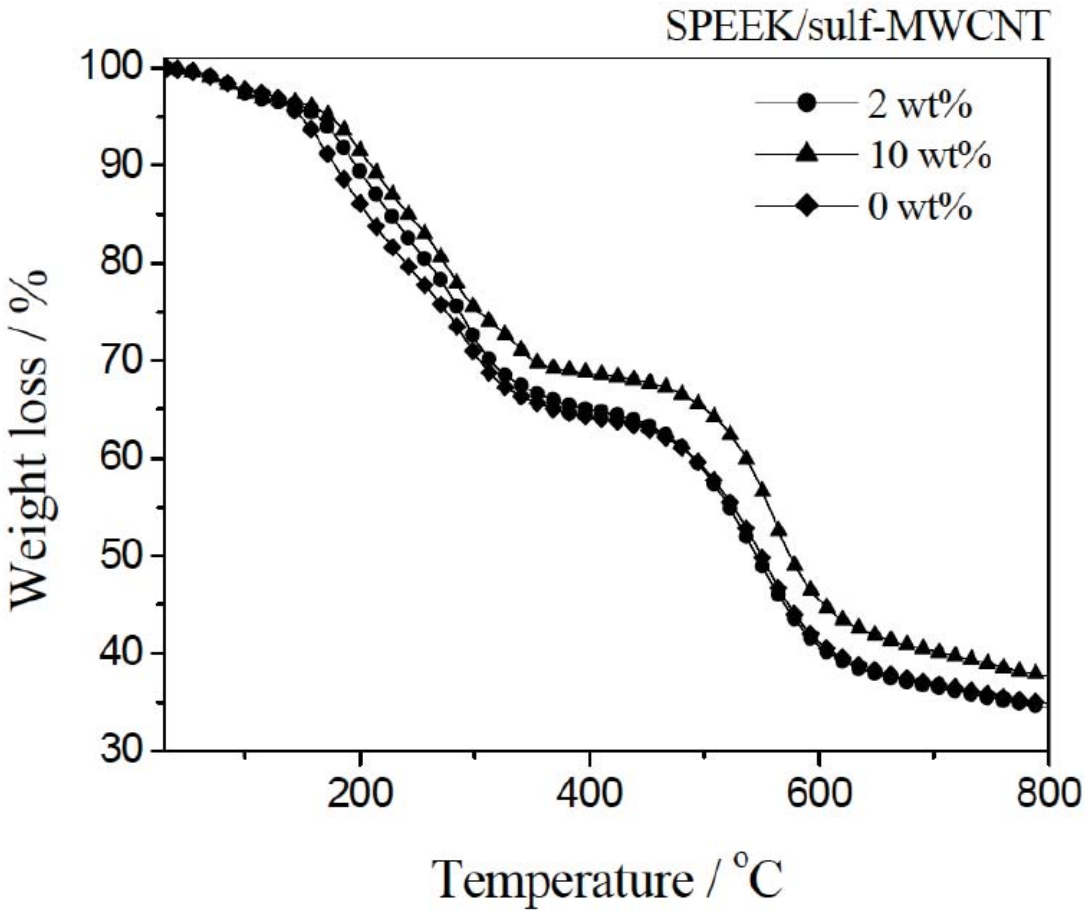

Figure 4. TGA of developed nanocomposite membranes.

Figure 5
Click here to download Figure(s): Figure 5.docx

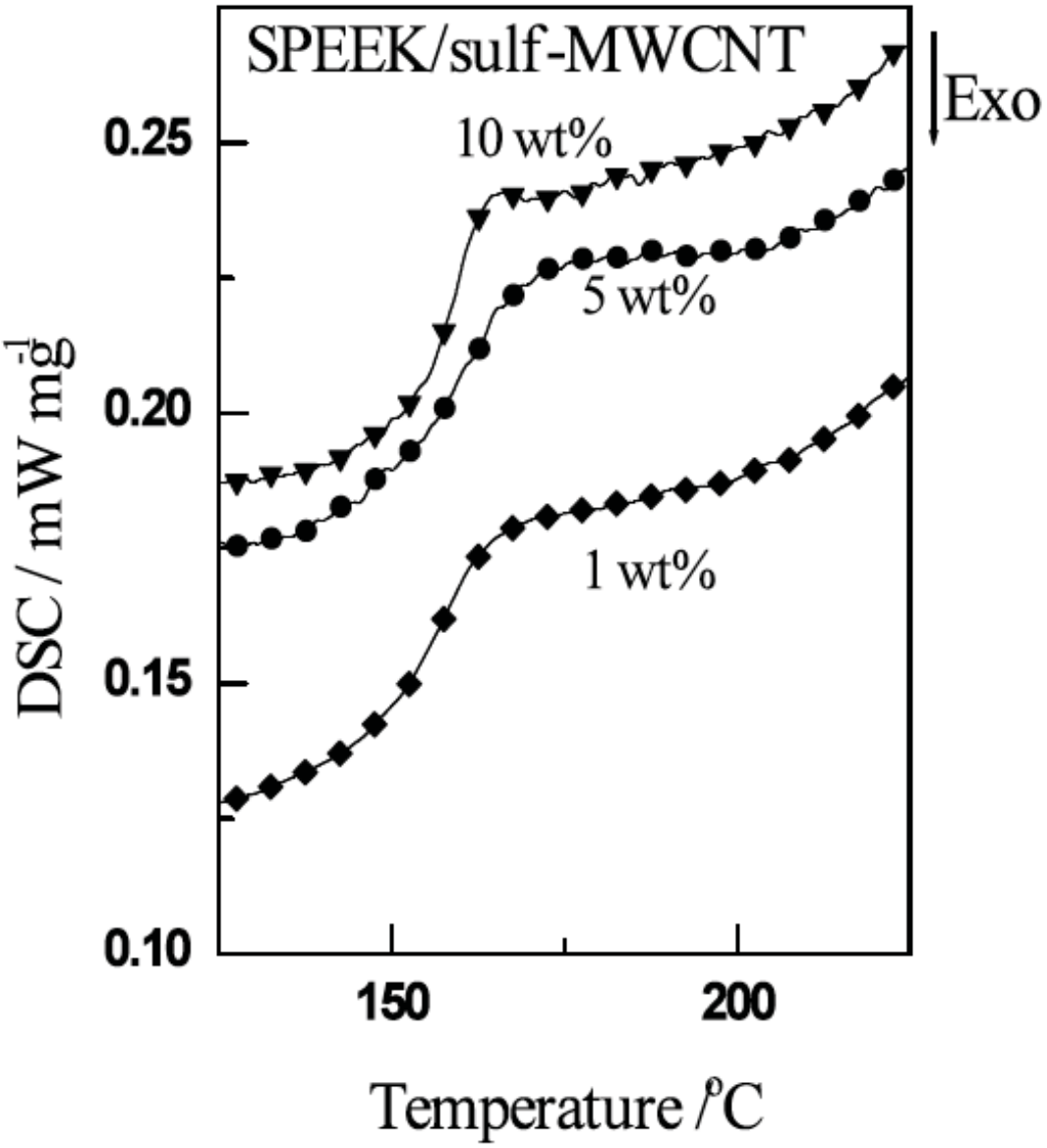

Figure 5. DSC of nanocomposite membranes.

Figure 6
Click here to download Figure(s): Figure 6.docx

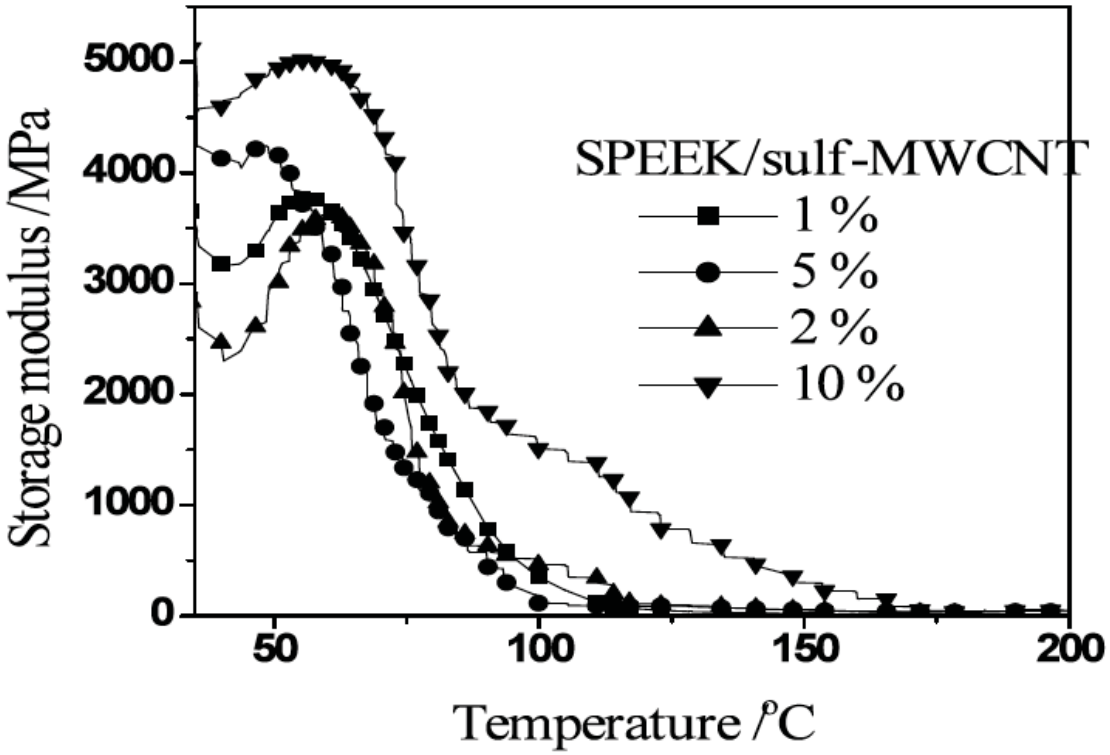

Figure 6. DMA curves showing the effect of sulf-MWCNT concentration on mechanical property.

Figure 7
Click here to download Figure(s): Figure 7.docx

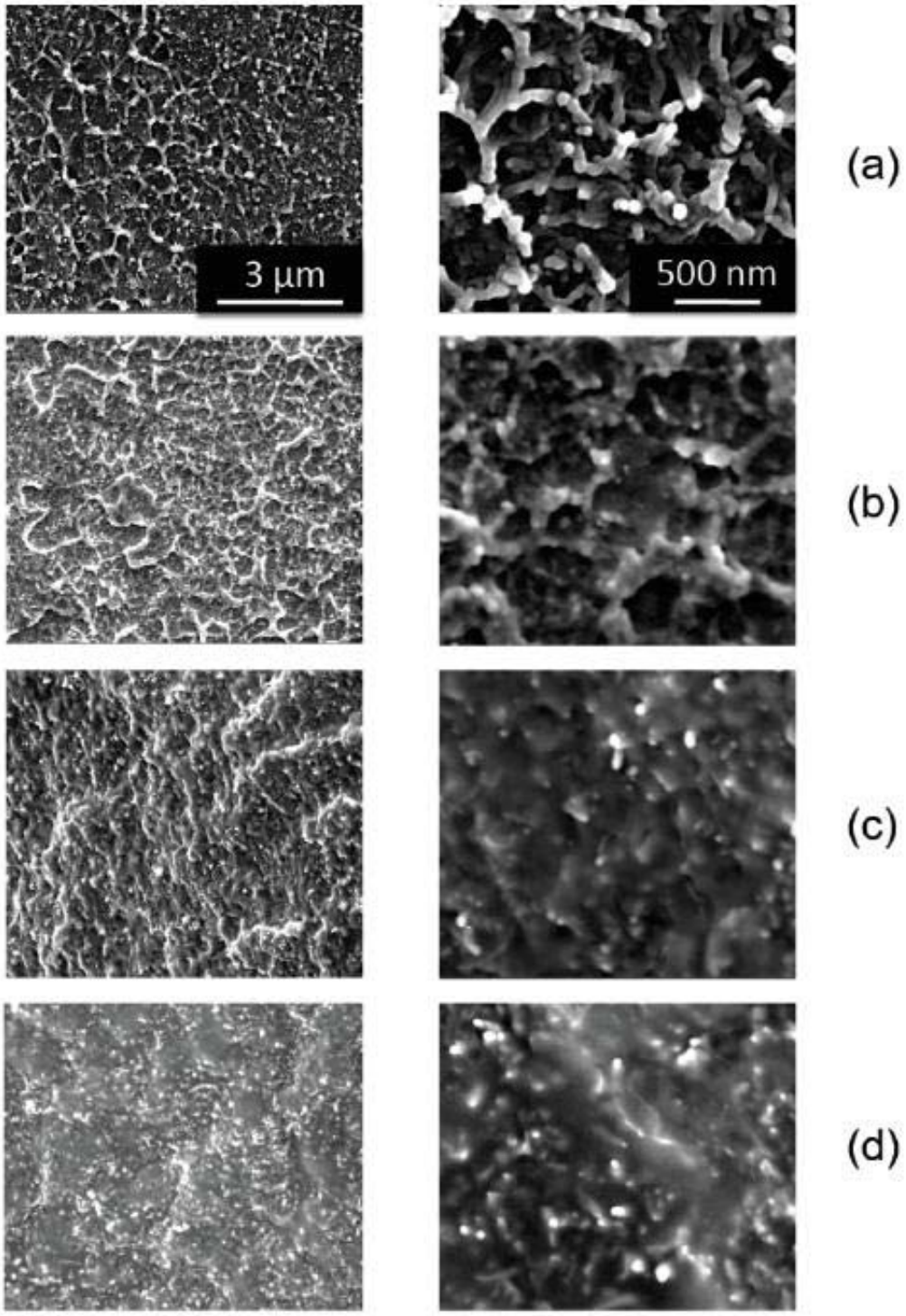

Figure 7. FESEM micrographs of SPEEKmembranes containing (a) non-functionalized MWCNT and (b) 1, (c) 5 and (d) 10 wt % sulf-MWCNT. Low (left) and high (right) magnification.

Figure 8
Click here to download Figure(s): Figure 8.docx

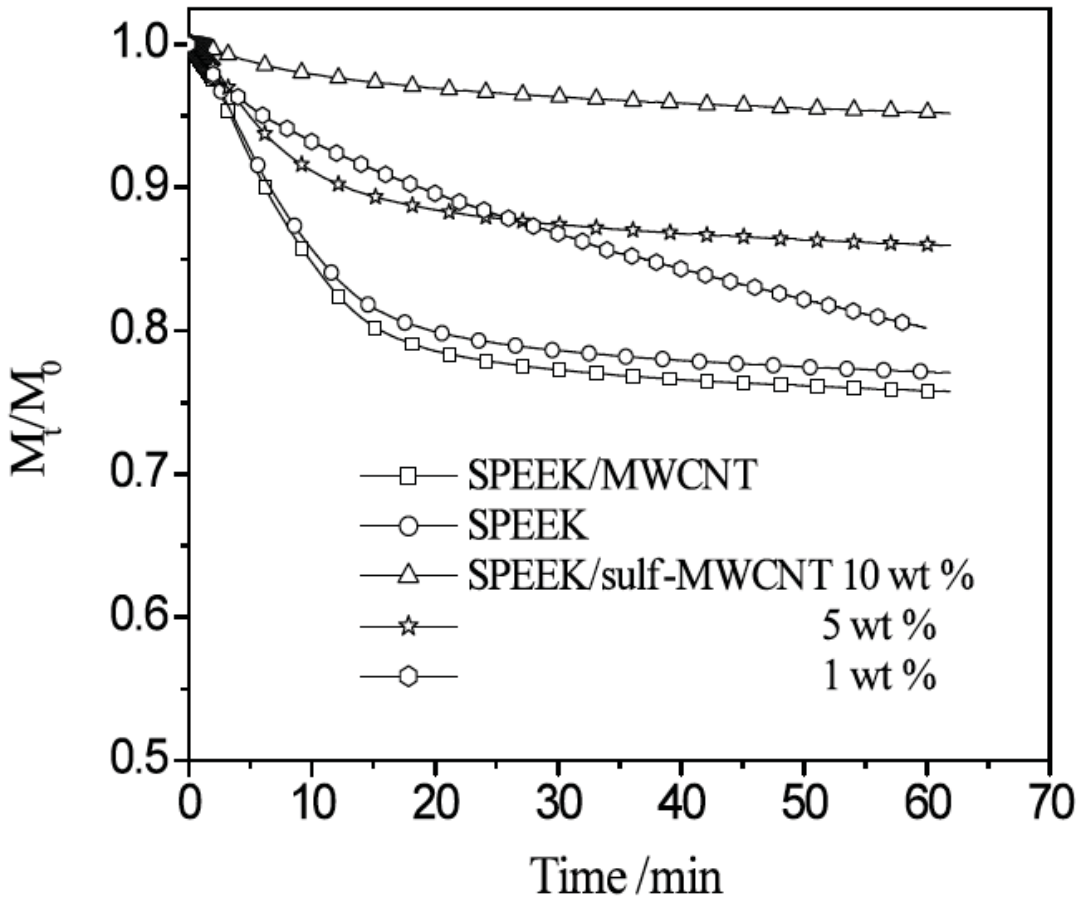

Figure 8. Water desorption profile for the nanocomposite membranes.

Figure 9
Click here to download Figure(s): Figure 9.docx

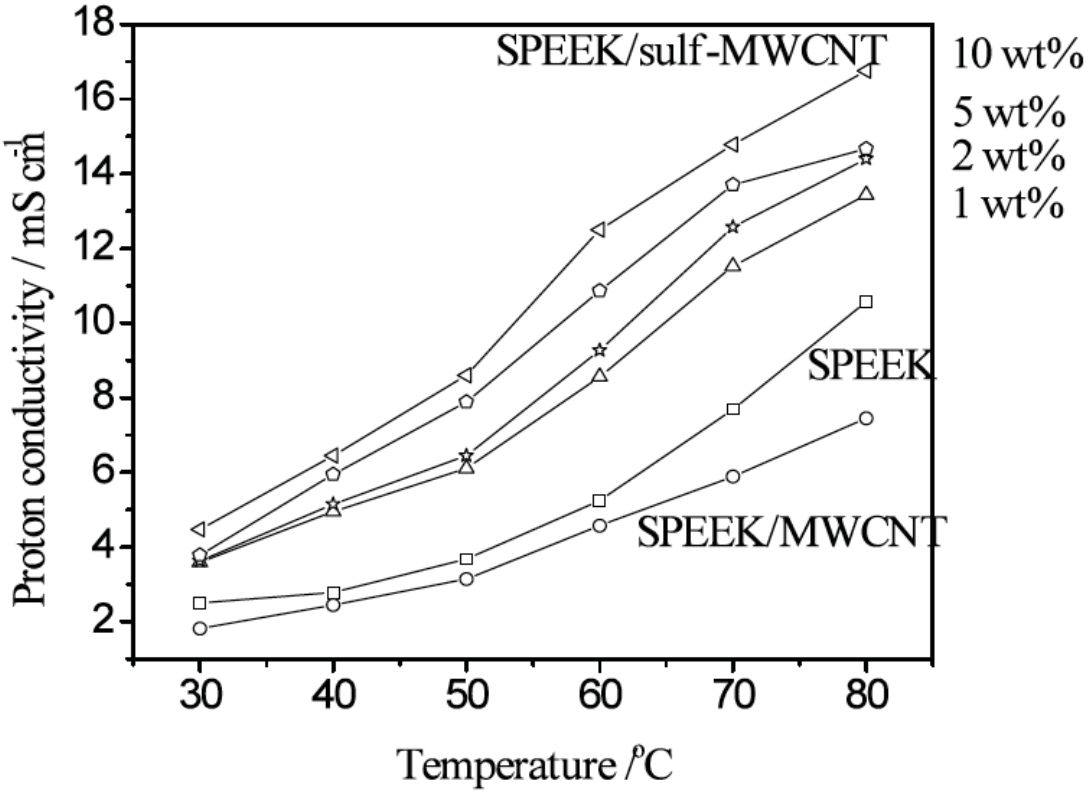

Figure 9. Proton conductivity of the developed membranes at different temperatures under 100% relative humidity.

Figure 10
Click here to download Figure(s): Figure 10.docx

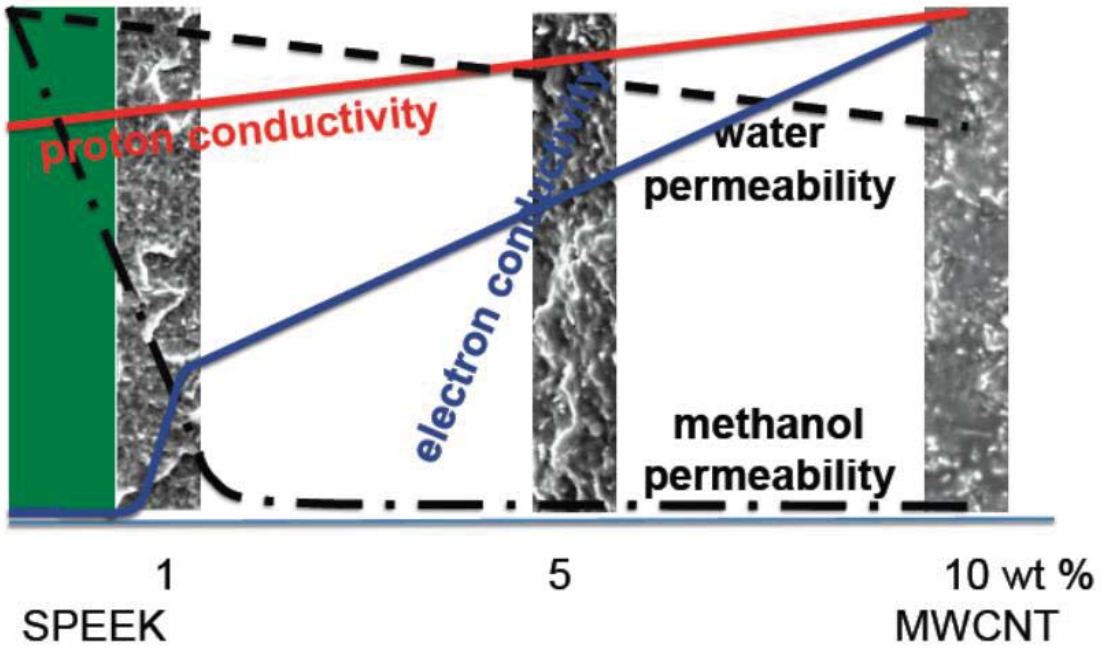

Figure 10. Influence of carbon nanotubes content on different membrane properties.